Preparation of polymeric particles in CO 2 medium using non-toxic solvents: discussions on the mechanism of particle formation

My-Kien Tran, Amin Swed, Brice Calvignac, Kim-Ngan Dang, Leila N. Hassani, Thomas Cordonnier, Frank Boury

Journal of Materials Chemistry B

PAPER

View Article Online
View Journal

Cite this: DOI: 10.1039/c4tb01319k

Preparation of polymeric particles in CO_2 medium using non-toxic solvents: discussions on the mechanism of particle formation†

My-Kien Tran,‡[ab] Amin Swed,‡[ab] Brice Calvignac,[ab] Kim-Ngan Dang,[ab] Leila N. Hassani,[ab] Thomas Cordonnier[ab] and Frank Boury*[ab]

Received 8th August 2014
Accepted 21st December 2014

DOI: 10.1039/c4tb01319k

www.rsc.org/MaterialsB

The aim of this work was to develop a novel formulation method, termed modified-PGSS (modified-Particle from Gas Saturated Solution), for the encapsulation of protein into polymeric microparticles in CO_2 medium. In this study, isosorbide dimethyl ether (DMI), a non-toxic water-miscible solvent, was used for the formulation and lysozyme was chosen as a model protein for encapsulation into PLGA microparticles. First, the mechanism of particle formation has been extensively studied and was discussed in detail. Phase behavior was investigated by measuring the solubility of CO_2 in DMI and volumetric expansion of DMI saturated in CO_2. Here, we demonstrate the consistency of the experimental values with the data obtained from the mathematical (such as the neural network) and thermodynamic (such as the Peng–Robinson equation of state) models. These models were built to develop predictive tools in the chosen experimental space for microparticle formulation. Furthermore, these microparticles were characterized in terms of size and zeta potential. The morphology and protein distribution within PLGA microparticles were determined using scanning electron microscopy and confocal microscopy, respectively. High encapsulation efficiency (65%) was obtained as confirmed by lysozyme quantification using a specific bioassay (*M. lysodeikticus*). Moreover, the *in vitro* protein release profile from loaded microparticles was presented. In this study, we report an innovative and green process for lysozyme encapsulation into PLGA microparticles. Thus, this process could be applied to the encapsulation of therapeutic proteins requiring protection and controlled release such as growth factors for regenerative medicine.

I. Introduction

The advances in biotechnology have allowed the production of biomolecules which have therapeutic actions in various research areas.[1,2] Even so, a major restriction still remains and limits their use at the clinical level. Indeed, their instability due to physical and chemical stresses has led researchers to find ways to protect these biomolecules and to control their release. To achieve this, carriers have been developed and among them polymeric particulate systems have attracted great attention for decades to protect and deliver biomolecules in many application fields.[3,4] An interesting example is the encapsulation of growth factors in such systems which offer a controlled release of these bioactive molecules for regenerative medicine.[5–8] Different encapsulation methods have been developed and can be used for protein encapsulation such as water/oil/water (w/o/w),[9] solid/oil/water (s/o/w),[10] simple coacervation[11] and spray-drying.[12] However, the common point of the above-mentioned methods is the use of toxic volatile solvents, which are harmful to the environment, patient health, and operators. Efforts to avoid the use of these solvents in encapsulation processes have been undertaken. For example, supercritical fluid and dense gas technology provides an interesting approach to completely eliminate these solvents or at least to minimize their use.[13] Actually, CO_2 is the most studied as a supercritical fluid or as a compressed gas in formulation processes since it is non-toxic, non-inflammable and environmentally friendly. In addition to its low cost, the mild critical conditions of CO_2 ($T = 304.25$ K and $P = 73.8$ bar) can be easily achieved. Therefore, supercritical or compressed CO_2-based processes are attractive technologies for protein encapsulation.[14–17] On the other hand, the use of low-toxic, high-boiling-point solvents such as dimethyl sulfoxide (DMSO),[18] glycofurol (GF)[19,20] and isosorbide dimethyl ether (DMI)[21] emerges as an alternative to classic solvents for the formulation of polymeric particles. To the best of our knowledge, DMI appears to be the

[a]LUNAM Université, Angers, France. E-mail: frank.boury@univ-angers.fr; Fax: +33 2 44 68 85 46; Tel: +33 2 44 68 85 28

[b]INSERM U1066, Micro-Nanomédecines Biomimétiques, IBS, 4 rue Larrey, F-49933 Angers Cedex 9, France

† Electronic supplementary information (ESI) available. See DOI: 10.1039/c4tb01319k

‡ These authors contributed equally to this work.

Table 1 Toxicity review of different water-miscible solvents

Solvent	LD_{50} (mL kg^{-1})[22]	Hemolytic activity[23]	Cardiovascular toxicity[24]	Angiotoxicity (duration of vasospasm)[25]
DMSO	6.9 (iv/m.) 12.6 (ip/m.) 15 (po/m.)	Very high	Moderate	19.1
NMP	4.4 (ip/m.)	Moderate	High	5.0
GF	3.5 (iv/m.)	Moderate	Insignificant	10.5
DMI	8.54 (iv/r.)	Low	Insignificant	5.9
PEG200	7.6 (iv/m.) 12.9 (ip/m.) 26 (po/m.)	High	Insignificant	—

safest solvent at the time being based on different toxicity criteria (Table 1). In a previous paper, a new procedure for the formulation of PLGA particles in CO_2 medium using DMI as the polymer solvent has been introduced and compared with a phase separation method.[21] In the present paper, we will focus on the understanding of the mechanism of particle formation. The solubility measurement showed that CO_2 is very soluble in DMI, which allows the DMI–CO_2 mixture to have tunable properties with pressure and temperature and to form an emulsion with an aqueous phase in CO_2 medium. Moreover, the relationship between the stirring rate and particle size will be shown to prove the existence of an emulsification step in our formulation method. The model protein (lysozyme) was encapsulated into PLGA particles to show proof-of-concept of our encapsulation method. Besides, *in vitro* release of the protein from PLGA microparticles was realized to validate the interest of loaded microparticles for sustained release. Using our new formulation method, it will be feasible to encapsulate therapeutic proteins such as growth factors. This original method could be very useful in tissue engineering for cell survival and differentiation and could also be extended to other biomedical fields.

II. Materials & methods

II.1. Materials

Lysozyme (chicken egg-white), *Micrococcus lysodeikticus*, isosorbide dimethyl ether (1,4:3,6-dianhydro-2,5-di-*O*-methyl-D-glucitol), Rhodamine B isothiocyanate (RITC) and Lutrol® F68 were obtained from Sigma-Aldrich (Saint Quentin Fallavier, France). Uncapped 75/25 PLGA provided by Phusis (Saint-Ismier, France) had a mean molecular weight of 21 000 Da (polydispersity index $I = 1.8$) as determined by size-exclusion chromatography (standard: polystyrene). CO_2 (purity of 99.995%) was obtained from Solfrance (Saint Ouenl'Aumone, France). Ethanol and acetonitrile (HPLC quality) were purchased from Fischer Scientific and trifluoroacetic acid (TFA, HPLC quality 37% w/w) was obtained from Carlo Erba, France. A filter of 0.2 μm for HPLC analysis was purchased from Acrodisc, PALL, USA. Phosphate buffered saline (PBS) was purchased from Lonza biowhittaker®, Belgium. Purified water was obtained from a Milli-Q® Advantage A10 system (Millipore, Paris, France). The micro-BCA protein assay reagent kit was purchased from Pierce (Bezons, France). All samples were lyophilized in a freeze-dryer (Lyovax GT, Steris®, France) for 18 hours.

II.2. Methods

II.2.1. Solubility of CO_2 in DMI

II.2.1.1. Measurement of the solubility of CO_2 in DMI. In this work, solubility measurements were carried out using a gravimetric method. The general principle of this method involves taking a sample of the DMI–CO_2 mixture without disturbing the thermodynamic equilibrium of this mixture. An experimental device was designed in order to achieve this objective (ESI,† Fig. 1). This type of device has been previously developed and employed for measuring the solubility of CO_2 in DMSO and in cocoa butter.[26,27] Briefly, the procedure of the measurements was composed of the following steps:

- The first step entailed obtaining an equilibrium state of the DMI–CO_2 mixture in a thermostatted cell (2) ($V = 94$ mL) provided with a mechanical stirrer.

- Once the pressure and temperature were stable, the valves V-5 and V-6 were opened to sample the DMI saturated with CO_2. Transfer was done in a thermostatted sampling cell (3) ($V \approx 5$ mL) which was subsequently weighed. Note that cell (2) was connected with a storage buffer cell (1) ($V = 300$ mL) which was used for the compensation of the pressure drop when sampling. Besides, all the pipes in the sampling loop were thermally controlled at the same temperature as that of the cells (1) and (2).

- The last step involved finding the mass of CO_2 in the mixture. In order to achieve this, a series of weighing operations, before and after CO_2 degassing, were carried out. The mass percentage of CO_2 in the mixture was calculated as in eqn (1).

$$X_{CO_2}(\%) = \frac{m_{DMI-CO_2} - m_{DMI}}{m_{DMI-CO_2}} \times 100 \quad (1)$$

where m_{DMI} is the mass of DMI in the mixture, while m_{DMI-CO_2} is the mass of the mixture sample.

II.2.1.2. Modeling of the solubility of CO_2 in DMI using a neural network. Measurements of the solubility of CO_2 in DMI were carried out under different conditions of pressure and temperature (ESI,† Fig. 2). Experimental points were selected to be well distributed in the experimental domain of pressure and

temperature, which makes the data suitable for further predictive modeling. In this paper, the neural network technique has been chosen for this purpose. Different topologies such as multi-layer perceptron (MLP), radial basis function (RBF), and generalized feed forward (GFF) have been tested using the same data set which had been randomized and partitioned into training, cross-validation and testing subsets in the same fashion. It appears that using MLP yielded the best performance. Hence, the MLP topology was chosen for further refinement. The leave-*N*-out approach (in this present paper, $N = 1$) was used to enhance the predictive quality by maximizing the use of data for training. In fact, the leave-*N*-out approach trains the network multiple times, each time omitting a different subset of data and using this subset for cross-validation, which is a good measure to show how well the model generalizes.[28] Besides, about 15% of the data was set aside to test the predictive quality of the obtained model and more importantly, to allow us to set an appropriate number of epochs to avoid overtraining the network. In reference to the architecture of the MLP topology, it was started with a low level of complexity with one hidden layer of three processing elements. The Levenberg–Marquardt method was chosen as the learning rule. Readers are referred elsewhere[29] for details of the algorithm and the calculation procedure. In this work, Neurosolution version 6 (Neurodimension, US) was used to create and train the neural networks. The performance of the chosen mathematical model is calculated according to eqn (2) and (3).

$$\mathrm{AAD} = \frac{1}{N}\sum_{i=1}^{N}\left|X_{\mathrm{cal}} - X_{\mathrm{exp}}\right| \tag{2}$$

$$\mathrm{AAD}(\%) = \frac{1}{N}\sum_{i=1}^{N}\frac{\left|X_{\mathrm{cal}} - X_{\mathrm{exp}}\right|}{X_{\mathrm{exp}}} \times 100 \tag{3}$$

where AAD is the average absolute deviation; X_{cal} and X_{exp} are respectively the calculated solubility and the experimental solubility.

II.2.1.3. Data correlation using an equation of state. In this part, experimental data on the solubility of CO_2 in DMI were correlated with the ϕ–ϕ approach using the Peng–Robinson equation of state (PR-EoS) with a standard alpha function. The equation for the Peng–Robinson model is as in eqn (4).

$$P = \frac{RT}{V_{\mathrm{m}} - b} - \frac{a}{V_{\mathrm{m}}(V_{\mathrm{m}} + b) + b(V_{\mathrm{m}} - b)} \tag{4}$$

A conventional mixing rule with an additional asymmetric term a_1 (ref. 30 and 31) was used to calculate the attractive and repulsive terms of the mixture as shown in eqn (5)–(14).

$$b = \sum_i x_i b_i \tag{5}$$

$$a = a_0 + a_1 \tag{6}$$

$$a_0 = \sum_i \sum_j x_i x_j (a_i a_j)^{0.5}(1 - k_{ij}) \tag{7}$$

$$k_{ij} = k_{ij}^{(1)} + k_{ij}^{(2)}T + k_{ij}^{(3)}/T \tag{8}$$

$$a_1 = \sum_{i=1}^{n} x_i \left(\sum_{j=1}^{n} x_j (a_i a_j)^{1/6} l_{ij}^{1/3}\right)^3 \tag{9}$$

$$l_{ij} = l_{ij}^{(1)} + l_{ij}^{(2)}T + l_{ij}^{(3)}/T \tag{10}$$

$$a_i = \alpha_i 0.45724 \frac{R^2 {T_{\mathrm{c}_i}}^2}{P_{\mathrm{c}_i}} \tag{11}$$

$$b_i = 0.07780 \frac{RT_{\mathrm{c}_i}}{P_{\mathrm{c}_i}} \tag{12}$$

$$\alpha_i = [1 + m_i(1 - {T_{\mathrm{r}i}}^{0.5})]^2 \tag{13}$$

$$m_i = 0.37464 + 1.54226\omega_i - 0.26992{\omega_i}^2 \tag{14}$$

where x_i, a_i, b_i, T_{ci}, P_{ci}, ω_i and T_{ri} respectively represent the mole fraction, attractive term, repulsive term, critical temperature, critical pressure, acentric factor and reduced temperature of component i, while k_{ij} and l_{ij} are the binary interaction parameters. The critical properties and acentric factor of the components were estimated using Joback's method[32] and their values are listed in the ESI,† Table 1.

For every component i in the mixture, the condition of thermodynamic equilibrium is given as shown in eqn (15).

$$f_i^{\mathrm{V}} = y_i \phi_i^{\mathrm{V}} P = x_i \phi_i^{\mathrm{L}} P = f_i^{\mathrm{L}} \tag{15}$$

where f_i^{V}, y_i, ϕ_i^{V} and f_i^{L}, x_i, ϕ_i^{L} represent the fugacity, mole fraction, and fugacity coefficient of component i in vapor and liquid phases. Readers may refer elsewhere[33,34] to find the form of $\ln \phi_i^{\mathrm{V}}$ and $\ln \phi_i^{\mathrm{L}}$ obtained from PR-EoS. The binary parameters were found by minimizing the Barker objective function for T-P-x data[35] according to eqn (16).

$$\psi = \sum_{j}^{n\,\mathrm{data}} \left(P_j - P_j^{\mathrm{calc}}\right)^2 \tag{16}$$

where n data are the total number of experimental points while P_j, P_j^{calc} are experimental and calculated pressures. Readers may refer to ref. 35 for more details on the mathematics of the regression technique. In this paper, Aspen Plus software (Aspen Technology, US) was used to perform the regression task and the estimation of physical properties.

II.2.2. Volumetric expansion measurement of DMI in CO_2 medium. The principle of the measurements involves measuring the volume change of DMI when put in contact with CO_2. Measurements were carried out in a thermostatted variable volume cell provided with sapphire windows, which made it possible to visually follow the volume change of DMI according to CO_2 pressure. The volumetric expansion was calculated according to eqn (17).

$$E\% = \frac{\left(V_{\mathrm{DMI-CO_2}} - V_{\mathrm{DMI}}^0\right) \times 100}{V_{\mathrm{DMI}}^0} \tag{17}$$

where V_{DMI}^0 and $V_{\mathrm{DMI-CO_2}}$ respectively represent the initial volume of DMI and volume of DMI–CO_2 mixture in the liquid

phase. In order to measure the volume increment, we carried out a calibration step under pressure with water (50 bar, 298.15 K). Water was chosen because of the weak solubility in CO_2 that involved a negligible volumetric expansion. Hence, calibration measurements consisted of determining the level of the liquid interphase which was correlated with the amount of water injected (ESI,† Fig. 3). The liquid level was determined by using image analysis software (ImageJ, NIH). The procedure of the volumetric expansion measurement was as follows: first, a precise initial volume of DMI was introduced into the cell; CO_2 was then delivered to the cell by means of a membrane pump; the mixture was subjected to mechanical stirring until pressure and temperature were constant; finally, the image of the liquid level in the cell was captured for image analysis and volume calculation. The volume inside the cell was known and could be modified any time, if necessary, to allow the liquid level to be observed *via* the sapphire window. Volume displacement was taken into account for the calculation of volumetric expansion. The maximal error of the level measurement was 4 pixels. The maximal error of volumetric expansion determination was approximately 3%.

II.2.3. Preparation of PLGA particles and lysozyme-loaded PLGA particles

II.2.3.1. Preparation of protein precipitates. Protein precipitation had been previously optimized using the experimental design.[21] Briefly, lysozyme was dissolved in 0.3 M NaCl solution at a concentration of 10 mg mL^{-1}. A volume of 90 μL of this solution was then mixed with 910 μL DMI, which in this instance played the role of an anti-solvent, to obtain a suspension of precipitated proteins for further use.

II.2.3.2. Formulation of PLGA particles in CO_2 medium. A scheme of the experimental setup used for the preparation of PLGA particles is shown in the ESI,† Fig. 4. First, 0.5 mL of a suspension of lysozyme precipitates in polymer solution was introduced into a 14 mL view-cell (E1), which was kept at the operating temperature (312.75 ± 0.1 K) by a thermostatted water bath. This suspension was prepared by adding 100 μL of lysozyme precipitates in DMI with 300 μL of polymer solution (7.5–20% w/v). This suspension was then gently mixed with 100 μL of ethanol to obtain the final 0.5 mL suspension to be introduced into the cell. In the case of preparing blank PLGA particles, 100 μL of protein precipitates were replaced by 100 μL of DMI. It should be noted that the use of 100 μL ethanol is warranted by the results obtained from the experimental design which had been previously carried out.[21] CO_2 was then delivered to the cell by means of a membrane pump. The mechanical stirring was carried out at 1050 rpm to favor the formation of an emulsion. Once the desired pressure (80 ± 0.1 bar) was reached, 1.5 mL of 6% w/v Lutrol® F68 solution (E2) was injected into the cell using a HPLC pump. Stirring was kept for 25 minutes before a depressurization step. A suspension of particles was then collected in (E3), which contained 5 mL of 6% Lutrol® F68 solution (solution E4). This suspension was left to stand for 30 minutes before 35 mL of solution E4 was added into it. The final suspension was kept at ambient temperature (≈298 K) for 8 hours. Thereafter, in order to collect the particles, the suspension was centrifuged at 2000*g* for 30 minutes. Particles were then washed once with distilled water before being freeze-dried. The supernatant was also stored for further quantification.

II.2.4. Particle characterization

II.2.4.1. Morphology. The surface morphology of the particles was investigated by scanning electron microscopy (SEM) (JSM 6310F, JEOL, Paris, France) at an accelerating potential of 3 kV. Freeze-dried microparticles were mounted onto metal stubs using double-sided adhesive tape and then vacuum-coated with a film of gold using a MED 020 (Bal-Tec, Balzers, Lichtenstein).

II.2.4.2. Particle size. The mean size and size distribution of microparticles were performed by the dynamic light scattering technique using a Mastersizer® Hydro 2000S (Malvern Instruments, Worcestershire, UK). The laser diffusion intensity is recorded as a function of the angle of diffusion; the size of particles and their repartition in number and volume can be assessed by the application of Fraunhofer diffraction and Mie scattering theories. Microparticles were suspended in purified water and used for these analyses. Results are an average of five measurements; a refractive index of 1.59 and absorption of 0.01 were used with a stirring rate of 1000 rpm with no ultrasound.

II.2.4.3. Zeta potential. Zeta potential was measured by the electrophoretic light scattering principle using a Nanosizer® ZS (Malvern Instruments, Worcestershire, UK). Microparticles suspended in purified water were used for these analyses. The results obtained are an average of five measurements.

II.2.4.4. Confocal microscopy. In order to visualize the distribution of lysozyme in the microparticles, lysozyme was labeled with RITC as described previously.[36] Briefly, 300 mg of lysozyme and 30 mg of RITC were incubated for 1 h at room temperature in a borate buffer at a pH of 9. After 1 h of reaction, the pH in the solution was reduced to 7.4 using 0.1 M boric acid. The solution was then transferred to a pre-swollen dialysis membrane tube (Spectra/Por®, MWCO 10 000) and lyophilized. The images of fluorescent microparticles were investigated using a confocal microscope Olympus Fluoview FV300 (Olympus, Japan). The software used for the CLSM imaging was Fluoview® Version 3.3 (Olympus, Japan) and for the acquisition 3D images, Imaris® (Bitplane, Switzerland).

II.2.5. *In vitro* release study

II.2.5.1. Determination of encapsulation yield. The total protein content was determined using micro-BCA assay. Briefly, the total amount of each batch (22.5–60 mg according to experiment conditions) of freeze-dried lysozyme-loaded PLGA particles was dissolved in 1.8 mL DMSO. After 1 h, 6 mL of HCl 0.01 M was added into the solution. The mixture was then incubated at 310.15 K (37 °C) overnight for the extraction of protein. After that, the mixture was centrifuged at 10 000*g* for 30 min. The transparent supernatant was then collected for quantification using a micro-BCA kit. The protein concentration was calculated using a standard curve after subtraction of the control value of the blank sample. The absorbance was measured at 580 nm with a Multiskan (Multiskan Labsystems, Thermo Fisher).

In this work, *M. lysodeikticus* was not used to quantify entrapped active protein because a possible overestimation of active protein may occur due to the presence of Lutrol® F68

adsorbed on PLGA particles. This method was only used to quantify the amount of active protein in the supernatant obtained after the formulation to correlate this one with the total protein determined by the micro-BCA method. The HPLC method was also used to compare with the micro-BCA method (*cf.* II.2.5.3).

II.2.5.2. Procedure of in vitro release. An *in vitro* release study was carried out using two approaches. In the first one, the entire batch of protein-loaded PLGA particles (22.5–60 mg depending on experimental conditions) was put into a centrifugation tube containing 6 mL of 0.0095 M (PO_4)–DPBS buffer, 0.1% w/v Lutrol® F68. The tube was incubated in a shaking water bath (310.15 K (37 °C), 125 rpm). In each tube, at determined intervals, the suspension of particles was centrifuged (30 min, 2000*g*) in order to collect the supernatant for further quantification. The total supernatant was then replaced by fresh buffer. The experiment was duplicated.

In the second approach, the *in vitro* experiment was carried out in a multiple-well plate (Transwell®, Corning). Each well contains an insert provided with a bottom porous membrane (polypropylene) (0.4 μm), which permits fluid exchange between inside and outside the insert. The suspension of protein-loaded PLGA particles was loaded into the insert. The buffer volumes inside and outside the insert were respectively 0.5 and 2 mL. Four wells were used to load the entire batch of particles. The plate was incubated in an oven at 310.15 K (37 °C) under a humid atmosphere in order to avoid dehydration, and was agitated using a rotating shaker at 290 rpm (Microtiter plate shaker SSM5, Stuart, UK). At determined intervals, the total outside volume was collected for quantification and totally replaced by fresh buffer. This experiment was duplicated.

II.2.5.3. Quantification of released protein. Active released protein was determined using *M. lysodeikticus*. Released-protein samples were diluted to an appropriate range of concentration before being incubated overnight with a suspension of *M. lysodeikticus*. Lysozyme activity determination was based on the turbidity measurement at 450 nm using a spectrophotometer (Shimadzu, Japan). Active protein was calculated using a standard curve.

Total protein released after 24 h was quantified using HPLC. HPLC assay was conducted using a PLRPS-Column (polymeric reversed phase Column; PLRP-S 250 4.6 mm, 300 Å pore size, 5 μm particle size; Agilent, Massy-France) followed by detection with a photodiode array detector (PDA 996, Waters Technologies, Guyancourt-France).[37] The system was equipped with a mobile phase delivery pump (600 Controller, Waters, Guyancourt-France), an auto sampler (Auto717 Plus, Waters, Guyancourt-France), an online degasser (AF, Waters, Guyancourt-France), and a column oven (Waters, Guyancourt-France) set at 318.15 K (45 °C). Typically, a filtered sample (50 μL) was injected into the column. The flow rate was 1 mL min^{-1}, and the mobile phase consisted of a gradient of water and acetonitrile both containing 0.1% v/v trifluoroacetic acid (TFA). Eluting conditions expressed as a proportion of water with 0.1% v/v TFA were as follows: 0–10 min: 69%, 19 min: 49.3%, 20 min: 25%, 20–21 min: 25%, 22 min: 69%, and 22–30 min: 69%. The lysozyme peak was identified in the chromatogram at a retention time of 20 ± 0.2 min. Besides, a UV spectrum was taken in order to confirm the identity of the peak and thus guarantee the specificity of the analysis. Lysozyme has a specific peak at 280 nm. The protein concentration was calculated based on a calibration curve.

III. Results & discussion

III.1. Solubility of CO_2 in DMI and volumetric expansion

In this work, the solubility of CO_2 in DMI was measured within a temperature range of 298.15 K to 318.15 K. The experimental results are summarized in the ESI, Table 2 and ESI,† Fig. 2. It can be seen that at a fixed pressure, the solubility of CO_2 in DMI decreases with increasing temperature. Remarkably, the solubility increases steeply with increasing pressure at a fixed temperature, which indicates the high solubility of CO_2 in DMI. For predictive purposes, a mathematical modeling step has been carried out using a neural network technique. Multi-layer perceptron topology with the leave-N-out training approach was used to train and test the network. Details of the network topology and training results can be found in the ESI,† Table 2. Fig. 1 shows experimental results and predicted data at 298.15 K, 313.15 K, and 318.15 K, for example. It can be seen that the established mathematical model fits very well with the experimental data. To get more insight into the behavior of DMI in CO_2 medium, experimental data were also correlated with the PR-EoSan. Results with values of temperature-dependent binary parameters obtained from regression are summarized in the ESI,† Table 3. The overall AAD% is 3.5%. It should be pointed out that the correlation may yield a better result by combining an advanced mixing rule based on a g^E model with Schwartzentruber–Renon–Watanasiri or Mathias–Copeman alpha function in which some polar terms are added. This approach has been proven to be more appropriate for polar components.[33,38] Moreover, it can be noted that Fischer and Gmehling[39] have made comparisons between several mixing rules based on predictive g^E models using Soave–Redlich–Kwong EoS to correlate the vapor–liquid equilibrium of a great variety of substances. The authors have shown that the error in pressure was about 2.5–3.5%, which is comparable with the results obtained in this work using a PR-EoS.

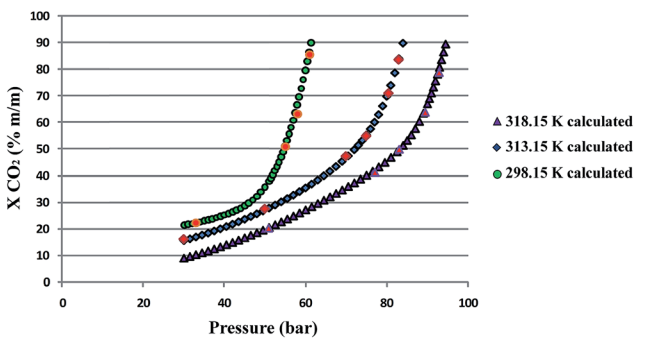

Fig. 1 Calculated and experimental solubilities of CO_2 in DMI. (●, ◆, ▲ and ●, ◆, ▲ are calculated and experimental data, respectively, at 298.15 K, 313.15 K, and 318.15 K.)

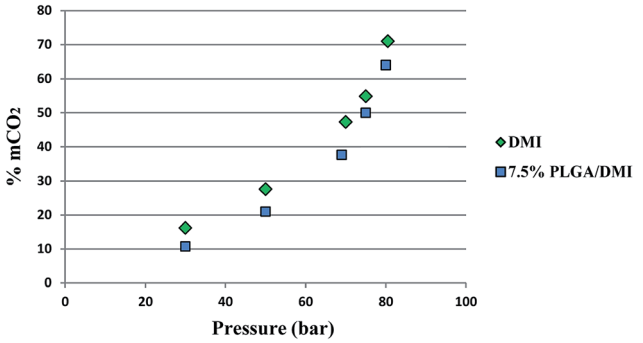

Fig. 2 Experimental solubility of CO_2 in polymer solution (7.5% PLGA/DMI) at 313.15 K.

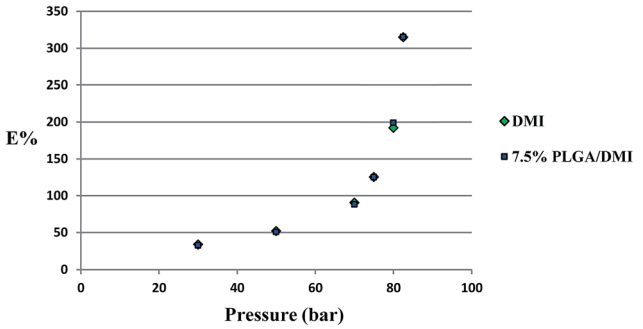

Fig. 3 Experimental volumetric expansion of DMI and polymer solution in CO_2 at 313.15 K.

Based on the prediction performance of the two above-mentioned approaches, we used the neural network model for routine calculations keeping in mind that the phenomenon can be explained well by thermodynamic equations. In the same way, measurements were carried out with a 7.5% w/v PLGA solution at 313.15 K (Fig. 2). It can be seen that the solubility of CO_2 in the polymer solution has the same profile as in DMI alone, which is highly pressure dependent at a fixed temperature. The solubility of CO_2 in PLGA/DMI is lower than in DMI alone, about 5–7 units at the same pressure. This fact can be attributed to the presence of PLGA in DMI which makes DMI less available for the interaction with CO_2. Moreover, it should be noted that at 313.15 K, the polymer solution of 7.5% PLGA begins to precipitate beyond 84 bar. Hence, at this temperature, the pressure conditions for the formulation of PLGA particles must be kept below this limit to prevent any prior precipitation of PLGA before the formation of an emulsion with an aqueous phase. Besides, the high solubility of CO_2 in DMI and PLGA/DMI can be also seen *via* a significant volumetric expansion (Fig. 3). The volumetric expansion is related to the solubility behavior according to CO_2 pressure at the fixed temperature. Volumetric expansion increases quickly, especially beyond 70 bar and it can reach up to about 200% at 80 bar.

III.2. Discussion on the mechanism of particle formation

In this work, we used the high solubility of CO_2 in DMI in order to form an emulsion composed of the DMI–CO_2 mixture with an aqueous phase as the first step of the formulation of PLGA particles. As already mentioned above, DMI is a water-miscible solvent, which makes it impossible to form an emulsion with an aqueous phase under atmospheric conditions. Therefore, it was decided to bring into play another component (CO_2), which interacts with DMI and water in a different way. Indeed, while CO_2 is barely soluble in water,[40] the solubility of CO_2 in DMI is very high as demonstrated above. The main idea behind this fact is that DMI saturated with CO_2 becomes less polar than DMI alone, which would slow down the diffusion of DMI into the aqueous phase and *vice versa*. This is the necessary condition for the formation of an emulsion. To have an idea on how the solubility of CO_2 influences the hydrophilic–hydrophobic character of the DMI–CO_2 mixture, the dielectric constant of the mixture was assessed. Based on Kirkwood theory[41] for a pure fluid, the dielectric constant ε is related to intermolecular interactions according to eqn (18).

$$\frac{(\varepsilon-1)(2\varepsilon+1)}{9\varepsilon}=\frac{4\pi N_A}{3\upsilon}\left(\alpha+\frac{\mu^2 g}{3kT}\right) \quad (18)$$

where α, μ, N_A, υ, and g respectively represent the molecular polarizability, dipole moment of the molecule, Avogadro's constant, molar volume, and correlation factor that characterizes the relative orientations between neighboring molecules. This equation can be rewritten to relate the polarization per unit volume of the fluid (p) to the dielectric constant as shown in eqn (19).

$$p=\frac{(\varepsilon-1)(2\varepsilon+1)}{9\varepsilon} \quad (19)$$

For the polarization of a mixture of n components, Oster's rule[41] can be applied according to eqn (20).

$$p_m=\frac{\sum_{i=1}^{n} x_i \upsilon_i p_i}{\sum_{i=1}^{n} x_i \upsilon_i} \quad (20)$$

where p_m is the polarization per unit volume of the mixture, while x_i, υ_i, and p_i are respectively the mole fraction, molar volume, and polarization per unit volume of pure component i.

Knowing that $p_{CO_2} < p_m < p_{DMI}$ and p is an increasing function of ε, the higher x_{CO_2} is, the more p_m approaches p_{CO_2} and the lower ε is. This fact led us to make a visualization test to study the miscibility between the polymer solution/DMI and water. Observation *via* a window sapphire shows a rather stable interface between the polymer solution and the aqueous solution (ESI,† Fig. 5). This indicates the possibility of forming an emulsion between the polymer solution and the aqueous solution in CO_2 medium. Hence, we sought to apply this result to the formulation of PLGA particles in CO_2 medium by using an emulsification–extraction method.

The best way to describe an emulsification process is to make time-series measurements of interfacial tension between dispersing and dispersed phases, which are water and CO_2-saturated DMI in this case. In this way, a high-pressure drop tensiometer is currently developed to carry out these

investigations and will be presented in a further study. In this work, to prove the existence of an emulsion in our formulation process, we chose to establish a relationship between the particle size and stirring rate. In fact, in an emulsification process, the particle size decreases as the stirring rate increases and *vice versa*. The particle size, which is the "fingerprint" of emulsion droplets formed during the process, was measured using the light scattering technique. A volume-weighted mean diameter D [4,3] of PLGA particles obtained after the formulation was selected to be investigated according to the variation of the stirring rate. The results combined with SEM images are summarized in Fig. 4. It clearly shows the relationship between the particle size and stirring rate, which strongly indicates the presence of an emulsion during our formulation process.

We termed our formulation method "modified-PGSS" (modified-Particles from Gas Saturated Solution) due to the fact that a CO_2-saturated polymer solution is called upon for the formation of an emulsion with an aqueous phase as the first step in the particle generation procedure. The polymer is dissolved beforehand in a water-miscible solvent. In this work, DMI, a high-boiling-point low-toxic solvent, is used for this purpose. After the first step of emulsion formation, CO_2-saturated solvent is slowly extracted to the dispersing phase, which is an aqueous solution, to allow the solidification of PLGA particles. Comparisons between classic PGSS and modified-PGSS for the generation of PLGA particles can be found in Table 2.

In the present work, the modified-PGSS process was used for lysozyme encapsulation. RITC-labeled lysozyme was encapsulated to allow further observation by confocal microscopy. The images of fluorescent PLGA particles can be found in Fig. 5A and B. A typical image of particles prepared by an emulsification method can be seen in Fig. 5A (2D slice image), which shows a polydisperse population of PLGA particles. Fig. 5B shows a zoom-in image of a RITC-lysozyme loaded PLGA particle after 3D reconstruction observed under an orthogonal view. It can be noted that RITC-lysozyme appears to be homogeneously distributed inside the particle. The proof-of-concept of our formulation method is hereby demonstrated. The SEM image, particle size, and zeta potential of lysozyme-loaded particles are shown in Fig. 6.

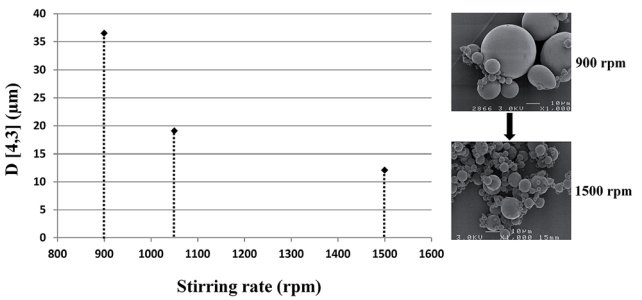

Fig. 4 Variation of the particle size according to the stirring rate.

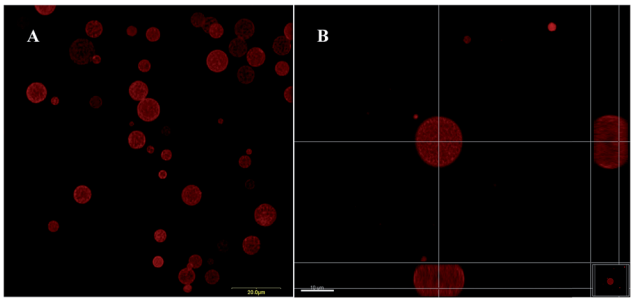

Fig. 5 Observations of RITC-lysozyme-loaded PLGA microparticles by confocal microscopy (A: 2D slice image; B: orthogonal view in *xy*, *xz*, and *yz* planes of a zoom-in particle after 3D reconstruction).

III.3. *In vitro* release study

The lysozyme encapsulation yield was about 65% quantified by micro-BCA and confirmed by the HPLC method. Moreover, active protein in the supernatant quantified by *M. lysodeikticus*, added up to the entrapped protein, was nearly equal to the initial amount of protein. *In vitro* release results after 14 days are shown in Fig. 7A. It should be noted that the total amount of protein released after 24 h quantified by HPLC equals to the amount of active protein quantified by *M. lysodeikticus*, which allows us to assume that the total protein entrapped into the particles also equals the active protein, which had not been directly quantified due to a possible overestimation in our case. The release study was carried out with different batches of particles prepared from polymer solutions at different concentrations. Whatever the starting concentration was, the release profile had a significant initial "burst" during the first day, followed by a slow-release phase. It can be seen that the lower polymer concentration is, the higher the burst release is. Due to the fast release during the first 24 h, it was decided to closely investigate the release profile in this period of time (Fig. 7B). It is hypothesized that lower polymer concentration results in a

Table 2 Comparison between classic-PGSS and modified-PGSS

Classic PGSS[13,42,43]	Modified-PGSS
Particle generation by spraying through a nozzle a CO_2-saturated solution of melted PLGA	Particle generation by emulsifying a CO_2-saturated PLGA solution with an aqueous phase
Without the use of organic solvents	PLGA is dissolved previously in water-miscible solvents (DMI, DMSO…)
Particle size is controlled by nozzle diameter, spraying rate…	Particle size is controlled by the stirring rate
Particle shape is irregular	Particle shape is spherical
Temperature $> T_{critical(CO_2)} = 304.25$ K	Temperature < or > $T_{critical(CO_2)}$

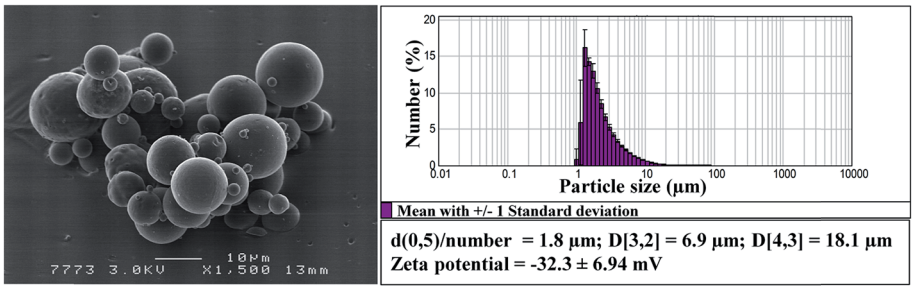

Fig. 6 SEM image of lysozyme-loaded particles and results of particle size and zeta potential analyses.

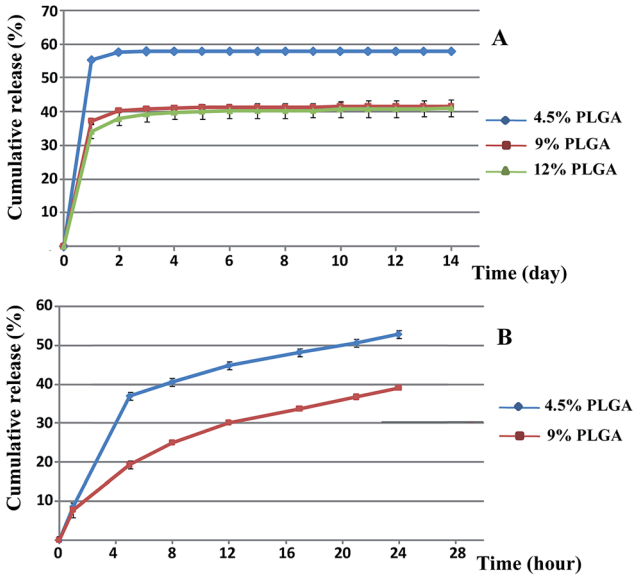

Fig. 7 *In vitro* release profile of lysozyme-loaded particles during 14 days (A) and during the first 24 h (B).

lower rate of solidification and thus leads to a faster release. These results are in agreement with those reported previously in the literature by other teams.[44,45]

After 14 days, PLGA particles were recovered and freeze-dried to quantify the remaining proteins. About 40% of remaining total protein was measured in each sample using the micro-BCA method. While the released active protein added up to the total remaining protein is equal to 100% in the case of 4.5% w/v PLGA, it is not the case for 9% and 12% w/v PLGA. This implies that about 20% of the protein was not revealed by dosing released active protein with *M. lysodeikticus*, which indicates that there was denatured protein in the release step in the case of 9% and 12% PLGA. In our preliminary work, it had been tested and proven that lysozyme is stable in the release medium (DPBS, 0.1% w/v Lutrol® F68). Hence, protein denaturation is believed to be related to protein interactions with the polymer. Such interactions could be non-specific adsorption to the polymer and ionic interaction with the uncapped carboxylic end-group.[46] Moreover, the acidic microenvironment inside PLGA particles can possibly affect the protein stability during incubation time as well.[46,47] Many suggestions have been made by different authors to overcome the protein instability within PLGA microparticles. For example, basic salts such as zinc carbonate and magnesium compounds were used to inhibit acid-induced protein degradation inside the microparticles during the *in vitro* release.[48,49] Furthermore, a PEGylated polymer or a blend of PEG and polymer was also proposed to reduce protein adsorption and to increase water uptake, thus favoring the release kinetics.[50,51] Moreover, surfactants such as poloxamers were incorporated into PLGA microparticles in order to enhance the stability and improve protein release.[7,52] These approaches are still under investigation.

In our laboratory, the obtained microparticles will be used to encapsulate growth factors and then combined with an injectable hydrogel for regenerative medicine. This combination aims to maintain the particles at the primary injection site to perform a local diffusion of the growth factors in order to improve recruitment and differentiation of the cell types involved in tissue regeneration. Therefore, the release profile established above may not be appropriate due to repetitive centrifugations that might accelerate the release rate. In addition, the presence of microparticles directly in contact with the total volume of release medium may not fit the reality where the release will take place nearby the injection site. Hence, the *in vitro* release was also carried out using another approach in which the suspension of microparticles was separated from the release medium by a porous membrane using a Transwell® system in order to avoid centrifugation steps and to better mimic the reality. The results are shown in Fig. 8.

Using this approach, it can be seen that the burst effect is clearly attenuated, which indicates that the release profile is

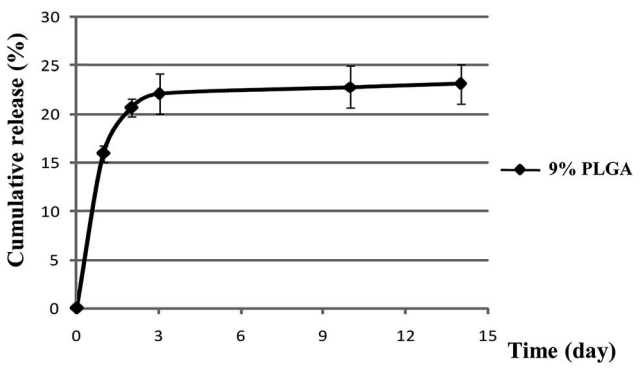

Fig. 8 *In vitro* release profile of lysozyme-loaded particles using the Transwell® approach.

strongly influenced by the technique employed in conducting the experiment. Moreover, there is no clear connection between *in vitro* conditions with the *in vivo* release profile. For instance, G. Jiang *et al.*[53] demonstrated that the release profile of lysozyme from PLGA particles (prepared by the w/o/w method) carried out in 0.1 M glycine–HCl buffer pH 2.5 had the best *in vitro*/*in vivo* correlation compared to other release media such as 0.1 M PBS pH 7.4 and 0.1 M acetate buffer pH 4.0. Therefore, until there is a standard procedure of *in vitro* experiment for protein-loaded PLGA particles, it would be difficult to make prediction from the *in vitro* release profile. *In vivo* studies are thus necessary to assess the release behavior of proteins in such a delivery system.

IV. Conclusions

In this work, we have discussed in detail the mechanism of polymeric microparticle formation in CO_2 medium, which is based on an emulsification–extraction process. DMI, as one of the safest injectable water-miscible solvents, was used for the formulation of PLGA particles. High encapsulation efficiency was obtained with preserved bioactivity of the encapsulated protein as confirmed by specific bioassay. The release profile could be improved by the incorporation of additives into the formulation. Although a model protein was chosen to be encapsulated to provide proof-of-concept, the encapsulation procedure presented in this paper can be extended to other fragile biomolecules including growth factors, thanks to the modeling of the CO_2 solubility in DMI, which allows particle formulation under mild conditions of pressure and temperature. In our laboratory, the use of such a sustained release system could be envisaged for tissue engineering purposes. Firstly, therapeutic proteins such as growth factors could be loaded within PLGA microparticles. Secondly, these carriers can be incorporated into a scaffold (*e.g.* an injectable hydrogel) containing adult stem cells for cartilage regeneration.

Acknowledgements

The authors thank the financial support of ANR (France—Project ANR-09-PIRI-0004-01), Regional research program (Pays de Loire, France—Bioregos program), the French and Syrian education ministers. We would like to thank the SCIAM ("Service Commun d'Imageries et d'Analyses Microscopiques") of Angers for scanning electron microscopy images.

References

1 D. Ibraheem, A. Elaissari and H. Fessi, *Int. J. Pharm.*, 2014, **459**, 70–83.
2 M. L. Tan, P. F. M. Choong and C. R. Dass, *Peptides*, 2010, **31**, 184–193.
3 C. E. Mora-Huertas, H. Fessi and A. Elaissari, *Int. J. Pharm.*, 2010, **385**, 113–142.
4 M. Ye, S. Kim and K. Park, *J. Controlled Release*, 2010, **146**, 241–260.
5 L. Lu, M. J. Yaszemski and A. G. Mikos, *TGF-β1 Release from Biodegradable Polymer Microparticles: its Effects on Marrow Stromal Osteoblast Function*, 2001.
6 C. Bouffi, O. Thomas, C. Bony, A. Giteau, M. C. Venier-Julienne, C. Jorgensen, C. Montero-Menei and D. Noel, *Biomaterials*, 2010, **31**, 6485–6493.
7 M. Morille, T. Van-Thanh, X. Garric, J. Cayon, J. Coudane, D. Noël, M.-C. Venier-Julienne and C. N. Montero-Menei, *J. Controlled Release*, 2013, **170**, 99–110.
8 A. Swed, T. Cordonnier, F. Fleury and F. Boury, *J. Nanomed. Nanotechnol.*, 2014, **5**, 2.
9 A. Aubert-Pouëssel, M.-C. Venier-Julienne, A. Clavreul, M. Sergent, C. Jollivet, C. N. Montero-Menei, E. Garcion, D. C. Bibby, P. Menei and J.-P. Benoit, *J. Controlled Release*, 2004, **95**, 463–475.
10 T. Morita, Y. Sakamura, Y. Horikiri, T. Suzuki and H. Yoshino, *J. Controlled Release*, 2000, **69**, 435–444.
11 C. Thomasin, H. P. Merkle and B. A. Gander, *Int. J. Pharm.*, 1997, **147**, 173–186.
12 B. Gander, P. Johansen, H. Nam-Trân and H. P. Merkle, *Int. J. Pharm.*, 1996, **129**, 51–61.
13 M. J. Whitaker, J. Hao, O. R. Davies, G. Serhatkulu, S. Stolnik-Trenkic, S. M. Howdle and K. M. Shakesheff, *J. Controlled Release*, 2005, **101**, 85–92.
14 M. K. Tran, L. N. Hassani, B. Calvignac, T. Beuvier, F. Hindré and F. Boury, *J. Supercrit. Fluids*, 2013, **79**, 159–169.
15 T. J. Young, K. P. Johnston, K. Mishima and H. Tanaka, *J. Pharm. Sci.*, 1999, **88**, 640–650.
16 K. Mishima, K. Matsuyama, D. Tanabe, S. Yamauchi, T. J. Young and K. P. Johnston, *AIChE J.*, 2000, **46**, 857–865.
17 P. Caliceti, S. Salmaso, N. Elvassore and A. Bertucco, *J. Controlled Release*, 2004, **94**, 195–205.
18 U. Bilati, E. Allémann and E. Doelker, *AAPS PharmSciTech*, 2005, **6**, E594–E604.
19 D. Allhenn and A. Lamprecht, *Pharm. Res.*, 2010, **28**, 563–571.
20 A. Aubert-Pouëssel, M.-C. Venier-Julienne, P. Saulnier, M. Sergent and J.-P. Benoît, *Pharm. Res.*, 2004, **21**, 2384–2391.
21 M.-K. Tran, A. Swed and F. Boury, *Eur. J. Pharm. Biopharm.*, 2012, **82**, 498–507.
22 P.-E. Le Renard, O. Jordan, A. Faes, A. Petri-Fink, H. Hofmann, D. Rüfenacht, F. Bosman, F. Buchegger and E. Doelker, *Biomaterials*, 2010, **31**, 691–705.
23 F. Mottu, M.-J. Stelling, D. A. Rüfenacht and E. Doelker, *PDA J. Pharm. Sci. Technol.*, 2001, **55**, 16–23.
24 M. F. Laurent A, R. Chapot, J. Q. Zhang, O. Jordan, D. A. Rüfenacht, E. Doelker and J. J. Merland, *PDA J. Pharm. Sci. Technol.*, 2007, **61**, 64–74.
25 O. Dudeck, O. Jordan, K. T. Hoffmann, A. F. Okuducu, K. Tesmer, T. Kreuzer-Nagy, D. A. Rufenacht, E. Doelker and R. Felix, *AJNR Am. J. Neuroradiol.*, 2006, **27**, 1900–1906.
26 B. Calvignac, E. Rodier, J.-J. Letourneau and J. Fages, *Int. J. Chem. React. Eng.*, 2009, **7**, A46.
27 B. Calvignac, E. Rodier, J.-J. Letourneau, M. Almeida dos Santos Pedro and J. Fages, *Int. J. Chem. React. Eng.*, 2010, **8**, A73.

28 *NeuroDimension Newsletter, NeuroSolutions Tip Box: Leave-N-out training*, Volume 6, No. 4, http://www.nd.com/newsletter/Newsletter_v6_4.html#6.
29 J. C. Principe, N. R. Euliano and W. C. Lefebvre, *Neural and Adaptive Systems: Fundamentals through Simulations*, Wiley, New York, 2000.
30 P. M. Mathias, H. C. Klotz and J. M. Prausnitz, *Fluid Phase Equilib.*, 1991, **67**, 31–44.
31 M. Solórzano-Zavala, F. Barragán-Aroche and E. R. Bazúa, *Fluid Phase Equilib.*, 1996, **122**, 99–116.
32 B. E. Poling, J. M. Prausnitz and J. P. O'Connell, in *Properties of Gases and Liquids*, ed. McGraw-Hill, 5th edn, 2001, ch. 2.
33 B. E. Poling, J. M. Prausnitz and J. P. O'Connell, in *Properties of Gases and Liquids*, ed. McGraw-Hill, 5th edn, 2001, ch. 8.
34 J. Gmehling, B. Kolbe, M. Kleiber and J. Rarey, *Chemical Thermodynamics for Process Simulation*, Wiley-VCH, 2012.
35 R. Schefflan, *Teach Yourself the Basics of Aspen Plus*, John Wiley & Sons, 2011.
36 E. S. Lee, K.-H. Park, D. Kang, I. S. Park, H. Y. Min, D. H. Lee, S. Kim, J. H. Kim and K. Na, *Biomaterials*, 2007, **28**, 2754–2762.
37 L. N. Hassani, F. Hindre, T. Beuvier, B. Calvignac, N. Lautram, A. Gibaud and F. Boury, *J. Mater. Chem. B*, 2013, **1**, 4011–4019.
38 B. K. Jürgen Gmehling, M. Kleiber and J. Rarey, in *Chemical Thermodynamics for Process Simulation*, Wiley-VCH, 2012, ch. 5.
39 K. Fischer and J. Gmehling, *Fluid Phase Equilib.*, 1995, **112**, 1–22.
40 L. W. Diamond and N. N. Akinfiev, *Fluid Phase Equilib.*, 2003, **208**, 265–290.
41 P. Wang and A. Anderko, *Fluid Phase Equilib.*, 2001, **186**, 103–122.
42 J. Hao, M. J. Whitaker, B. Wong, G. Serhatkulu, K. M. Shakesheff and S. M. Howdle, *J. Pharm. Sci.*, 2004, **93**, 1083–1090.
43 L. Casettari, E. Castagnino, S. Stolnik, A. Lewis, S. Howdle and L. Illum, *Pharm. Res.*, 2011, **28**, 1668–1682.
44 Y. Y. Yang, T. S. Chung, X. L. Bai and W. K. Chan, *Chem. Eng. Sci.*, 2000, **55**, 2223–2236.
45 C. Yan, J. H. Resau, J. Hewetson, M. West, W. L. Rill and M. Kende, *J. Controlled Release*, 1994, **32**, 231–241.
46 U. Bilati, E. Allémann and E. Doelker, *Eur. J. Pharm. Biopharm.*, 2005, **59**, 375–388.
47 A. Giteau, M. C. Venier-Julienne, A. Aubert-Pouëssel and J. P. Benoit, *Int. J. Pharm.*, 2008, **350**, 14–26.
48 O. L. Johnson, W. Jaworowicz, J. L. Cleland, L. Bailey, M. Charnis, E. Duenas, C. C. Wu, D. Shepard, S. Magil, T. Last, A. J. S. Jones and S. D. Putney, *Pharm. Res.*, 1997, **14**, 730–735.
49 G. Z. Zhu, S. R. Mallery and S. P. Schwendeman, *Nat. Biotechnol.*, 2000, **18**, 52–57.
50 A. Lochmann, H. Nitzsche, S. von Einem, E. Schwarz and K. Mäder, *J. Controlled Release*, 2010, **147**, 92–100.
51 V.-T. Tran, J.-P. Karam, X. Garric, J. Coudane, J.-P. Benoît, C. N. Montero-Menei and M.-C. Venier-Julienne, *Eur. J. Pharm. Sci.*, 2012, **45**, 128–137.
52 A. Paillard-Giteau, V. T. Tran, O. Thomas, X. Garric, J. Coudane, S. Marchal, I. Chourpa, J. P. Benoît, C. N. Montero-Menei and M. C. Venier-Julienne, *Eur. J. Pharm. Biopharm.*, 2010, **75**, 128–136.
53 G. Jiang, B. H. Woo, F. Kang, J. Singh and P. P. DeLuca, *J. Controlled Release*, 2002, **79**, 137–145.

